Title: Soybean CHX protein GmSALT3 confers leaf Na^+ exclusion via a root derived mechanism, and Cl^- exclusion via a shoot derived process

Yue Qu[1†], Rongxia Guan[2†], Jayakumar Bose[1], Sam W. Henderson[1], Stefanie Wege[1*], Lijuan Qiu[2*], Matthew Gilliham[1*]

[1]Australian Research Council Centre of Excellence in Plant Energy Biology, School of Agriculture, Food and Wine & Waite Research Institute, University of Adelaide, Glen Osmond, SA, Australia

[2]The National Key Facility for Crop Gene Resources and Genetic Improvement, Institute of Crop Science, Chinese Academy of Agricultural Sciences, Beijing, China

[*]For correspondence (e-mails matthew.gilliham@adelaide.edu.au; qiulijuan@caas.cn; stephanie.wege@adelaide.edu.au).

[†]These authors have contributed equally to this work.

Funding information

Natural Science Foundation of China, grant number 31830066; Scientific Innovation Project of Chinese Academy of Agricultural Sciences; ARC Centre of Excellence funding CE140100008; ARC Fellowships FT130100709, DE160100804 and DE170100346.

Abstract

Soybean (*Glycine max*) yields are threatened by multiple stresses including soil salinity. *GmSALT3* confers net shoot exclusion for both Na^+ and Cl^- and improves salt tolerance of soybean; however, how the ER-localised GmSALT3 achieves this is unknown. Here, GmSALT3's function was investigated in heterologous systems and near-isogenic lines that contained the full-length *GmSALT3* (NIL-T; salt-tolerant) or a truncated transcript *Gmsalt3* (NIL-S; salt-sensitive). GmSALT3 restored growth of K^+-uptake-defective *E. coli* and contributed toward net influx and accumulation of Na^+, K^+, and Cl^- in *Xenopus laevis* oocytes, while *Gmsalt3* was non-functional. A time-course analysis of the NILs confirmed that shoot Cl^- exclusion breaks down prior to Na^+ exclusion, while grafting showed that shoot Na^+

exclusion occurs via a root xylem-based mechanism. In contrast, NIL-T plants exhibited significantly greater Cl^- content in both the stem xylem and phloem sap compared to NIL-S, indicating that shoot Cl^- exclusion likely depends upon novel phloem-based Cl^- recirculation. NIL-T shoots grafted on NIL-S roots contained low shoot Cl^-, which confirmed that Cl^- recirculation is dependent on the presence of GmSALT3 in shoots. Overall, these findings provide new insights on GmSALT3's impact on salinity tolerance and reveal a novel mechanism for shoot Cl^- exclusion in plants.

Highlight

GmSALT3 improves soybean salt tolerance. Here, using heterologous expression, we found GmSALT3 is a functional ion transporter, and, *in planta* that it confers shoot salt exclusion through root-based Na^+ xylem exclusion and shoot-based Cl^- exclusion via phloem derived Cl^- recirculation.

Keywords: Salinity tolerance, abiotic stress, soybean, GmSALT3, CHX, ion transporter, shoot ion exclusion

Acknowledgments:

This work was funded by the Natural Science Foundation of China, grant number 31830066 (RG); Scientific Innovation Project of Chinese Academy of Agricultural Sciences (LQ). YQ and SH were supported by ARC Centre of Excellence funding awarded to MG (CE140100008). ARC Fellowships supported MG (FT130100709), SW (DE160100804) and JB (DE170100346). We thank Yue (Crystal) Wu for generating the *AtCBL1n* entry vector; Dr. Sunita Ramesh and Assoc. Prof Zhonghua Chen for providing *AtKAT1* construct used in this study; Dr. Gwenda Mayo from Adelaide Microscopy for providing assistance in TEM.

Word count: 6654 (Abstract, Introduction, Methods, Results, Discussion, Acknowledgements)

Introduction

There is a large market demand for soybean (*Glycine max*) as a staple edible oil and food crop; soybean is also an important component of intercropping and sequential cropping systems (Singh, 2010). As such, soybean production demand has been projected to increase by nearly 80 percent to 390 Mt by 2050 (Alexandratos & Bruinsma, 2012). However, salinity stress threatens soybean production. A soil salinity of EC (electrical conductivity) 18–20 dS/m, which is approximately 180 – 200 mM NaCl, has been shown to reduce yield by 61% from 2261 ± 438 kg/ha under control conditions to 881 ± 260 kg/ha (Chang, Chen, Shao, & Wan, 1994). In another study, Blanco et al. (2007) found that the emergence of soybean (cv. Conquista) was completely inhibited when EC was close to 8.0 dS/m. Yet, natural variation in soybean salinity tolerance has been observed, with some rare soybean germplasm found to be relatively salt-tolerant. In a large-scale evaluation of soybean salinity tolerance, less than 3% of the 10,128 evaluated soybean germplasm exhibited salt tolerance at both the germination and seedling stage; only 83 soybean cultivars were found to have significant tolerance to salinity at the vegetative stage (Shao, Wan, Chang, & Chen, 1993). It has been observed that salt-tolerant soybean cultivars often have superior agronomic performance to salt-sensitive cultivars (Phang, Shao, & Lam, 2008), indicating breeding for stress tolerance in soybean may improve overall yields even under standard conditions.

In soybean, a major quantitative trait locus (QTL) for salinity tolerance (*Ncl*) has been consistently mapped to chromosome 3 (Abel, 1969; Ha et al., 2013; Hamwieh et al., 2011; Hamwieh & Xu, 2008; Lee et al., 2004). Since 2014, several studies have been published focusing on the same dominant gene within this QTL on chromosome 3, in both wild (*GmCHX1*) and cultivated soybean (*GmNcl*/*GmSALT3*) (Do et al., 2016; Guan et al., 2014; Qi et al., 2014). This gene, denoted as *Glyma03g32900* in the reference soybean genome of the William 82 variety (William 82. a1.v1.1), is the premier candidate for conferring improved salt tolerance in the *Ncl* locus. It should be noted that in the William 82 genome a2.v1, *Glyma03g32900* appears to be incorrectly annotated as two transcripts (Glyma.03g171600 and Glyma.03g171700) rather than the full-length coding sequence obtained consistently from cDNA and encoding a full-length CHX protein. Here, we refer to the full-length gene obtained as *GmSALT3*.

According to phylogenetic analyses, the full-length GmSALT3 protein is a member of the CPA2 (Cation/Proton Antiporter 2) family of transporters; the most closely related sequence in *Arabidopsis thaliana* being AtCHX20 (a Cation/Proton Exchanger) (with 59%

93 identity and 72% similarity) (Guan et al., 2014; Padmanaban et al., 2007). Several Arabidopsis
94 CHXs, including AtCHX20, have been functionally characterised in heterologous systems;
95 however, a connection to their function to roles in plants has been challenging, as examples of
96 phenotypes associated with loss of function mutations is sparse (Sze & Chanroj, 2018).
97 Functional studies of AtCHX have indicated that they might play role in modulating cation and
98 pH homeostasis within the endomembrane system (Chanroj et al., 2011; Czerny et al., 2016;
99 Padmanaban et al., 2007). The endomembrane localised AtCHX20 was, for example,
100 suggested to be a K^+ transporter involved in the osmoregulation of guard cells (Padmanaban et
101 al., 2007).

102 In soybean, the salt-tolerant soybean cultivar Tiefeng 8 contains a full-length *GmSALT3*,
103 while the salt sensitive cultivar 85-140 contains a 3.78-kb copia retrotransposon insertion in
104 exon 3 of *GmSALT3* that truncates the transcript with a premature stop codon (making the 85-
105 140 essentially a *Gmsalt3* knockout). This retrotransposon insertion resulted in the loss of the
106 10th predicted transmembrane domain and the C-terminus of *GmSALT3* (Guan et al., 2014).
107 *GmSALT3* is predominantly expressed in cells associated with the phloem and xylem (Guan et
108 al., 2014); and expression of the full-length *GmSALT3*, but not the truncated version, results in
109 low shoot Na^+ and Cl^- accumulation in saline conditions (Guan et al., 2014; Liu et al., 2016;
110 Qi et al., 2014). This low shoot NaCl accumulation is associated with increased crop yield (Do
111 et al., 2016; Liu et al., 2016). The GmSALT3 protein has been localized to the endoplasmic
112 reticulum (ER), sharing the membrane localisation of AtCHX20 in guard cells. This differs
113 from most other transport proteins known to be involved in shoot Na^+ and Cl^- exclusion, which
114 are mainly localised on the plasma membrane or tonoplast (Munns and Gilliham, 2015).

115 Shoot salt exclusion requires the co-ordinated activity of many ion transporters that
116 may: 1) limit the net entry of salt into the roots, 2) compartmentalise salt in the roots; and or 3)
117 regulate vascular transport (most notably through root-based xylem exclusion) (Munns et al.
118 2020). Examples of transporters that have been implicated in salt tolerance in soybean include:
119 the tonoplast localised GmNHX1 (Na^+/H^+ antiporter 1) (Li et al., 2006a), the plasma membrane
120 localised GmSOS1 (salt overly sensitive 1, Na^+/H^+ antiporter) and the plasma membrane
121 localised GmCAX1 (Ca^{2+}/H^+ antiporter 1) (Luo et al., 2005; Phang et al., 2008). These
122 transporters are proposed to be involved in net exclusion of salt entry into roots (GmSOS1),
123 salt compartmentation (*GmNHX1*) or signalling (*GmCAX1*). GmSALT3, was the first example
124 of a transporter contributing to reduced net transfer of salt to the shoot in soybean (Cao, Li,
125 Liu, Kong, & Tran, 2018). In other crop species, modulation of vascular ion load is commonly
126 found to be one of the major salt tolerance mechanisms. For instance, in wheat, rice and

127 Arabidopsis the HKT1;5-like (high affinity K^+ transport) proteins are expressed in xylem
128 parenchyma cells and facilitate Na^+ retrieval from xylem sap back into the root (Munns et al.,
129 2012; Møller et al., 2009; Ren et al., 2005; Uozumi et al., 2000). GmSALT3 differs from these
130 previous proteins; the ER-localised is unlikely to directly retrieve from or load ions into the
131 xylem sap. Therefore, GmSALT3 confers a novel salt tolerance mechanism which is yet to be
132 determined.

133 Here, we investigated the function of GmSALT3 in heterologous systems and *in planta*
134 to gain insights into the mechanisms by which GmSALT3 contributes to salt tolerance. In
135 heterologous systems, *GmSALT3* complemented K^+ uptake deficient *Escherichia coli*; while
136 in *Xenopus laevis* oocytes, *GmSALT3* expression resulted in increased net influx of Na^+, K^+
137 and Cl^-. Phenotypes of soybean NILs differing in *GmSALT3* alleles revealed that plants
138 containing full-length *GmSALT3,* compared to truncated *Gmsalt3,* employ two distinct
139 mechanisms to achieve shoot Na^+ and Cl^- exclusion by facilitating net xylem retrieval of Na^+
140 and a novel mechanism of greater phloem Cl^- retranslocation from shoots to roots. As such,
141 we propose that the endomembrane GmSALT3 has a complex physiological role which
142 ultimately impacts multiple ion fluxes across the plasma membrane.
143

144 **Materials and Methods**

145 *Plant materials and growth conditions*

146 Soybean plants were grown in a greenhouse (28 °C day, 16 h light and 25 °C night) at
147 the Plant Research Centre, Waite Campus, University of Adelaide, Australia. Soybean seeds
148 (Tiefeng 8, salt-tolerant parent; 85-140, salt-sensitive parent; NIL-T, near isogenic line with
149 *GmSALT3*; NIL-S, near isogenic line with *Gmsalt3*) were imported from China through
150 quarantine. Soybean seeds were germinated in pots containing a 1:1 mixture of
151 perlite:vermiculite as described by Obermeyer & Tyerman (2005), with no nutrient solution
152 added.
153

154 *cDNA cloning and plasmid preparation*

155 To synthesize *GmSALT3* and *Gmsalt3* cDNA (2436 and 1131 nucleotides, respectively),
156 total RNA was isolated from roots of 4-week old soybean plants using the TRIzol method (Shi
157 & Bressan, 2006). First-strand cDNA was synthesized using a Thermoscript RT III kit
158 (Invitrogen, USA). Gene specific primers (GmSALT3_gF and GmSALT3_gR, Gmsalt3_gF
159 and Gmsalt3_gR; Table S1) were used to amplify *GmSALT3* cDNA with Phusion® High-

160 Fidelity DNA Polymerase (New England Biolabs) using 35 cycles (98 °C 30 s, 65 °C 30 s, and
161 72 °C 150 s). Gel-purified PCR products were A-tailed using Taq polymerase (New England
162 Biolabs) for 30 min at 72 °C, and then recombined into Gateway® entry vector
163 PCR8/GW/TOPO (Invitrogen) for subsequent applications. Resulting clones were sequenced
164 using internal primers (GmSALT3_F1, R1, F2, F3, F4, and F5, Gmsalt_F1, F2, and R1; Table
165 S1). The sequence of *GmSALT3-YFP* was PCR amplified from a previously constructed
166 plasmid *pBS-35S::GmSALT3-YFP*; the sequence of *GmSALT3-TM10* (first 10 transmembrane
167 domain of *GmSALT3*) was PCR amplified from *PCR8-GmSALT3*. Gel-purified PCR products
168 of *GmSALT3-YFP, GmSALT3-TM10* were recombined into entry vector PCR8 as described
169 above.
170 *GmSALT3* and *Gmsalt3* CDS, *GmSALT3-YFP, GmSALT3-TM10, AtCHX20 and*
171 *AtKAT1* within entry vector PCR8 were cloned into the pGEM-HE vector and a modified
172 version of pET-DEST42 vector using Gateway ® LR Clonase® (Invitrogen, USA), for *X. laevis*
173 oocyte expression and *E. coli* expression, respectively. The *E. coli* strain TK2463 lacks the T7
174 RNA polymerase, therefore, the T7 promoter in pET-DEST42 was replaced with the TAC
175 promoter. Inverse PCR was performed with 5 ng of plasmid, 50 nM of forward and reverse
176 primer (SH_215 and SH_216, Table S1), and 0.25 units Phusion High Fidelity Polymerase
177 (New England Biolabs) in a final volume of 25 µL. Reactions were treated with Cloning
178 Enhancer (Clontech Laboratories Inc) to remove circular template, and the plasmid was re-
179 circularised using In-Fusion HD enzyme (Clontech Laboratories Inc).
180
181 *Growth assay in Escherichia coli*
182 Competent cell preparation and *E. coli* transformation were conducted as described by
183 Chanroj et al. (2011). The resulting transformants were grown on KML media (10 g/L tryptone,
184 5 g/L yeast extract, 10 g/L KCl) supplemented with 100 µg/mL carbenicillin and incubated at
185 37 °C overnight; positively transformed colonies were identified by colony PCR with gene
186 specific primers (GmSALT3_gF and _gR; Gmsalt3_gF and gR). For *E. coli* growth
187 experiments, freshly transformed cells were first grown overnight in 5 ml KML at pH 7.2. Cell
188 cultures were replenished (OD_{600} = 0.5) and grown for 3 h in KML, and then washed with low
189 potassium media (10 g/L tryptone, 2 g/L yeast extract, 100 mM D-mannitol) three times. Cells
190 were normalized to OD_{600} 0.5 for a 96-well plate assay. In each well, 20 µL of normalized cell
191 suspension was added to 180 µL growth solutions. All test media were supplemented with 100
192 µg/mL carbenicillin, with or without 0.5 mM IPTG (Isopropyl β-D-1-thiogalactopyranoside).
193 The 96-well plates were inserted into FLUOstar Omega Fluorescence microplate reader (BMG

194 LABTECH) set to 37 ºC and A_{600} was measured every 15 min for 18 h with continuous shaking
195 at 200 rpm.
196
197 *Characterization of GmSALT3 in X. laevis oocytes*
198 pGEMHE-DEST containing *GmSALT3* was linearized using SphI-HF (New England
199 BioLabs); cRNA was synthesized using mMESSAGE mMACHINE T7 Kit (Ambion). 46
200 nL/23 ng of cRNA or equal volumes of RNase-free water were injected into oocytes with a
201 Nanoinject II microinjector (Drummond Scientific). Oocytes were incubated for 48 h in
202 Calcium Ringer's solution (96 mM NaCl, 2 mM KCl, 5 mM $MgCl_2$, 5 mM HEPES, 0.6 mM
203 $CaCl_2$). All solution osmolalities were measured with a Vapor pressure osmometer (Wescor)
204 and adjusted to 240–260 mOsmol kg^{-1} using mannitol. Measurement of ion profiles in oocytes
205 followed Munns et al. (2012) with the following modifications. Six replications of 3 grouped
206 oocytes were used for flame photometry (Sherwood 420), and Cl^- was measured by manual
207 titrimetric Cl^- measurement using a chloride analyser (Sherwood® Chloridometer 926S). For
208 YFP imaging, oocytes were analysed with a Zeiss LSM 5 Pascal Confocal Laser-Scanning
209 Microscope equipped with an argon laser. Excitation/emission conditions for YFP were 514
210 nm/523-600 nm.
211
212 *Ion-selective microelectrode flux measurements from oocytes*
213 The MIFE™ (Microelectrode Ion Flux Estimation technique; University of Tasmania, Hobart,
214 Australia) allows noninvasive concurrent quantification of net fluxes of several ions using
215 protocols outlined by Shabala et al. (2013) with oocytes being used rather than plant tissues in
216 our experiments. Potassium and chloride commercial ionophore cocktails (99311, and 99408,
217 respectively; all from Sigma-Aldrich) were used as LIX (Liquid Ion Exchanger) when
218 measuring K^+ and Cl^- fluxes. The Na^+ fluxes were measured using an improved Na^+ LIX
219 described in Jayakannan et al. (2011). Oocytes were washed in ND96 (96 mM NaCl, 1 mM
220 KCl, 1 mM $MgCl_2$, 5 mM HEPES, pH 7.5). After incubation in ND96 for 72 hours, fluxes
221 were measured after being transferred to BSM (5 mM NaCl, 0.2 mM KCl, 0.2 mM $CaCl_2$, 5
222 mM HEPES, pH 7.5). During measurements, the ion-selective electrodes were positioned using
223 a 3D-micromanipulator (MMT-5, Narishige, Tokyo, Japan), 100 µm from the oocyte surface.
224 A computer-controlled stepper motor moved the electrode between two positions (100 and 200
225 µm, respectively) from the oocyte surface in 6 s cycles. The CHART software (Newman, 2001)
226 recorded the potential difference between the two positions and converted them into

227 electrochemical potential differences using the calibrated Nernst slope of the electrode. Net ion
228 fluxes were calculated using the MIFEFLUX software for spherical geometry (Newman, 2001).
229
230 *TEM (Transmission Electron Microscopy)*
231 Fresh soybean NIL-T and NIL-S roots were sectioned to 1 mm (length), stems were
232 cross sectioned (1 mm in length and 1 mm in radius). Root and stem samples were incubated
233 overnight in 1.5 ml microcentrifuge tubes with fixative (2.5% Glutaraldehyde, 4%
234 Formaldehyde, 4% Sucrose, 0.1 M Phosphate buffer). Samples were washed three times in 1X
235 PBS and then washed with osmium (263257, Sigma-Aldrich) for 4 hours. Sections were then
236 washed three times in 1X PBS and soaked in 1X PBS for 20 mins and then embedded in a 1%
237 agarose gel. Agarose embedded soybean root were cut into blocks (1 cm long). A series of
238 dehydration steps were performed after embedding, using increasing concentrations of ethanol:
239 50%, 70%, 90% and 95% (each for 30 mins), and 100% ethanol for overnight dehydration.
240 Samples were then incubated in increasing concentrations of resin (Spurrs): 5%, 10%, 15%,
241 20%, 25%, 30%, 40%, and 50% (each for 1 h), 50% overnight, 75% (4 h), 100% (4 h), and
242 100% (overnight). Resin wells containing the agarose blocks were then incubated at 60 ^{o}C for
243 3 days for polymerization. Polymerised resin capsules were cut to 70 nm thickness using a
244 diamond knife and visualized under transmission electron microscopy (TEM; PHILIPS
245 CM100).
246
247 *NaCl treatment and ion accumulation*
248 Soybean plants were treated with 100 mM NaCl every 2 days (1.5 L solution per tray)
249 at 14 days after sowing; the second dose of 1.5 L 100 mM NaCl was applied 16 days after
250 sowing; the same volume of RO (reverse osmosis) water was applied to the tray of the control
251 plants. Plant tissues were harvested and dried in an oven overnight at 60°C or freeze-dried
252 overnight. Dry weight was recorded, then dried samples were digested in 10 mL 1% (v/v) nitric
253 acid overnight at 65°C or freeze-thawed in Milli-Q water 3 times. Oven-dried samples were
254 utilized to test Na^+ and K^+ accumulation with flame photometry (Sherwood 420), Cl^- was
255 measured by titrimetric Cl^- measurement by using a chloride analyser (Sherwood®
256 Chloridometer 926S).
257 Freeze-dried samples were used to measure NO_3 accumulation. The measurement
258 method was modified according to Qiu, Henderson, Tester, Roy, & Gilliham (2016).
259 Supernatant (50 µL) of freeze-dried samples in water was added into 200 µL of 5% (W/V)
260 salicylic acid/H_2SO_4 and incubated at room temperature for 20 min, then 50 µL of this mixture

261 was transferred into 950 µL of 2 M NaOH and incubated at room temperature for at least 20
262 min (to cool down to room temperature). Of this, 250 µL was loaded into separate wells of a
263 flat-bottom transparent 96-well plate (Greiner Bio-One, Austria). Absorbance was measured
264 at 410 nm. Standards measured included 0, 0.5, 1, 2, 2.5, 5, 7.5, and 10 mM KNO_3.
265
266 *Phloem and xylem sap extraction*
267 Phloem sap was extracted according to the method of Rupassara (2008) and Ren et al.
268 (2005). Soybean and stems were cut approximately 2 cm above the ground level with the upper
269 part immediately dipped in 1.5 mL of 0.1 mM EDTA solution (pH adjusted to 8 with NaOH)
270 in a 2 mL microcentrifuge tube for 20 min, then the tube was immediately dipped in liquid
271 nitrogen and stored in -80ºC until analysis. The glutamine concentration in the extract was
272 measured using a Glutamine Assay Kit (EGLN-100, EnzyChrom™, BioAssay Systems).
273 Xylem sap was extracted using a pressure chamber. Lower parts of the cut stems with roots
274 were transferred into the pressure chamber. Pressure was increased gradually (0.05 MPa
275 increments) until the xylem sap presented. The first two drops emerging were discarded using
276 a micropipette to reduce contamination from damaged cells or phloem sap (Berthomieu et al.,
277 2003). Xylem sap was then collected during the following 5 min, and stored at -20 ºC until
278 analysis. Ion contents was measured as stated above.
279
280 *Grafting of soybeans*
281 NIL-T and NIL-S were grown in a growth chamber with a 16 h light (28 °C)/8 h dark
282 (25 °C) cycle at 60% humidity. The grafting protocol followed Guan *et al.* (2014) with the
283 following modifications. After grafting, when the first trifoliate leaf fully expanded (about 10
284 days after grafting), healthy plants were selected and treated with 100 mM NaCl for 8 days.
285 Na^+, K^+, and Cl^- contents were measured in soybean leaves and roots.
286
287 **Results**
288 *GmSALT3 expression impacts Na^+, K^+, and Cl^- fluxes in heterologous systems*
289 We functionally characterised GmSALT3 in heterologous systems, including *E. coli*
290 and *X. laevis* oocytes. The *E. coli* strain TK2463 (*trkAΔ, kup1Δ, kdpABCDEΔ*) is defective in
291 its native K^+ uptake mechanisms (Epstein, Buurman, McLaggan, & Naprstek, 1993) (Fig. 1)
292 and shows a reduced growth trajectory in low K^+ media (Epstein et al., 1993). We transformed
293 TK2463 bacteria with our constructs of interest and controls; expression of the proteins was

294 driven by the IPTG (Isopropyl β-D-1-thiogalactopyranoside)-inducible tac-promoter. In low
295 K^+-containing medium (~2 mM K^+), expression of full length *GmSALT3* improved growth
296 compared to expression of truncated *Gmsalt3*, and the negative control (AtCBL1n, a 12 aa
297 peptide with the sequence MGCFHSKAAKEF; Batistič, Waadt, Steinhorst, Held, & Kudla,
298 2010) (Fig. 1a; 1b). Arabidopsis AtCHX20 (Chanroj et al., 2011) and AtKAT1 (Anderson,
299 Huprikar, Kochian, Lucas, & Gaber, 1992), a known plasma membrane potassium channel
300 from Arabidopsis, were included as positive controls and restored bacteria growth as expected
301 (Fig. 1a; 1b). We had previously used GmSALT3-YFP for determining the subcellular
302 localisation of GmSALT3 (Guan et al., 2014), and therefore investigated if this translational
303 fusion is functional and could complement TK2463 *E. coli*. Additionally, we were interested
304 whether the last transmembrane domain of GmSALT3 is important for functionality - truncated
305 *Gmsalt3* from NIL-S contains only 9 out of the 10 predicted alpha-helices. We therefore
306 constructed GmSALT3-TM10, that has all 10 TM alpha -helices with only the large (383 aa)
307 hydrophilic C-terminus removed. Both, YFP-tagged GmSALT3 and GmSALT3-TM10
308 increased *E. coli* growth to that of GmSALT3, and significantly greater than that of Gmsalt3
309 (Fig. 1a; 1b). None of the test constructs or controls had a significant impact on bacterial growth
310 rates on high K^+ media (Fig. S1c-d); or showed significant differences on low K^+ media without
311 IPTG-induction (Fig. S1a-b). In addition, we measured K^+ content of *E. coli* cells, to determine
312 the impact of *GmSALT3* expression on K^+ accumulation. Bacteria were grown for 12 h in low
313 K^+ following IPTG induction, and then harvested. Results indicated that expression of full
314 length *GmSALT3* leads to higher K^+ content in bacteria, as does expression of *GmSALT3-YFP,*
315 *GmSALT3_TM10, AtKAT1,* and *AtCHX20* (Fig. S1e). Expression of truncated *Gmsalt3* resulted
316 in similar low K^+ content as in the negative control.
317 We chose a second heterologous expression system to investigate if the ER-localised
318 GmSALT3 impacts the fluxes of ions additional to K^+. We expressed YFP-tagged and
319 untagged GmSALT3, as well as Gmsalt3, in *X. laevis* oocytes and detected fluorescence at the
320 PM in GmSALT3-YFP expressing oocytes, similar to the PM-localised positive control
321 TmHKT1;5-A-YFP (Fig. 2a) (*Triticum monococcum* High-Affinity K^+ Transporter 1; Munns
322 et al., 2012). This indicates that GmSALT3-YFP localises to the PM in oocyte, which is
323 different from its ER-localisation in plant cells (Guan et al., 2014). It is not uncommon for
324 plant endomembrane proteins to at least partially localise to the PM in frog oocytes (Maurel,
325 Reizer, Schroeder, & Chrispeels, 1993; Henderson et al., 2015); however, this restricts the
326 interpretation of the data regarding the impact of ER-localised transporters on PM ion fluxes.

327 Two electrode voltage-clamp electrophysiology revealed that the resting membrane potential
328 of GmSALT3-injected oocytes was more positive compared to H_2O-injected oocytes when
329 incubated in ND96 media (Fig. 2b), but no consistent current differences were detected. This
330 suggests that transport through GmSALT3 might be electroneutral, which is consistent with
331 the CPA2 signature sequence for electroneutral ion transport (Masrati et al., 2018). Therefore,
332 we chose to conduct MIFE (Microelectrode Ion Flux Estimation) experiments to measure the
333 net fluxes of specific ions across the plasma membrane of oocytes non-invasively and so does
334 not rely upon net charge movement in a particular direction.
335 Flux analysis indicated that in *GmSALT3*-injected oocytes net efflux of Na^+, K^+, and
336 Cl^- was reduced compared to H_2O-injected oocytes (Fig. 2c). Subsequent ion content analysis
337 of oocytes revealed that *GmSALT3*-injected oocytes contained significantly more K^+, Na^+, and
338 Cl^- compared to H_2O-injected oocytes, in agreement with the reduced net ion efflux in oocytes
339 (Fig. 2d). To test whether the GmSALT3 induced differences in ion concentration could be
340 blocked, we used the Na^+ channel and Na^+/H^+ exchanger inhibitor amiloride hydrochloride
341 (Darley et al., 2000). Oocytes were transferred from ND96 to BSM (low Na^+, K^+ and Cl^-) and
342 incubated overnight with or without the inhibitor. *GmSALT3*-injected oocytes incubated
343 without amiloride, showed a smaller relative K^+, Na^+, and Cl^- decrease in compared to H_2O-
344 injected oocytes as expected (Fig. 2d). In the presence of amiloride, however, this difference
345 was not observed (Fig. 2d), strongly suggesting that GmSALT3 affects the transport of K^+, Na^+,
346 and Cl^- across the PM in oocytes. Collectively, the heterologous data has advanced our
347 knowledge by confirming that *GmSALT3* encodes a competent transport protein, certainly
348 capable of transporting K^+, and affects the flux of Na^+, K^+ and Cl^- across a plasma membrane.
349 However, as it is unclear whether the net fluxes of Na^+, K^+ and Cl^- across the plasma membrane
350 of oocytes were all carried directly by GmSALT3, rather than endogenous *X. laevis* transport
351 proteins we focused our efforts on further characterising the impact of GmSALT3 on salt
352 transport *in planta*.
353
354 *GmSALT3 modulates Na^+, K^+, and Cl^- accumulation in soybean*
355 Liu et al. (2016) previously used an extreme salt treatment (200 mM NaCl) screen that
356 typically results in the death of even the more salt tolerant germplasm after a prolonged
357 exposure. Using this method, it was observed that full-length *GmSALT3* improved shoot Na^+
358 and Cl^- exclusion over 10 days, with higher shoot Cl^- accumulation occurring prior to shoot
359 Na^+ accumulation in NIL-S (Liu et al., 2016). Here, we used a lower salt concentration (100
360 mM) that soybean plants are more likely to encounter in the field, and which typically does not

361 result in death of the plants prior to seed production. Furthermore, we studied the time course
362 of Na^+, Cl^- and K^+ accumulation in NIL-T and NIL-S for different leaf types, stems and
363 hypocotyls (Fig. 3). We confirmed that Cl^- accumulates to higher concentrations in NIL-S
364 shoots compared to those of NIL-T (Fig. 3b). Even without a salt treatment Cl^- concentration
365 was found to be greater in NIL-S aerial tissues (leaves and stems), whereas significantly higher
366 Na^+ accumulation was detected in aerial tissues only after 3 days of NaCl treatment in NIL-S,
367 with Cl^- being even more pronounced as time after salt treatment progressed (Fig. 3a,b; Fig.
368 S2, S3). We further observed that the K^+/Na^+ ratio was significantly higher in NIL-T leaves
369 compared to NIL-S when measured after day 3 (Fig. 3d). Total K^+ content was increased in
370 NIL-S compared to NIL-T (Fig. 3c; Fig. S3), but K^+ accumulation increased to lesser extent
371 compared to Na^+ accumulation. K^+ increased from 35.7±1.2 mg/g (day 0) to 51.2±1.2 mg/g
372 (day 10), compared to 0.3±0.1 mg/g and 45.3±5.6 mg/g for Na^+ in the same period (Fig. 3a;
373 3c). Therefore, although shoot K^+ increased in NIL-S, the K^+/Na^+ ratio was lower. In addition,
374 salt treatment affected biomass production and after 10 days NaCl treatment the total dry
375 weight of NIL-T was significantly higher, as were individual dry weights of leaves, roots, and
376 stem (Fig. 3e, f).

377 After establishing the timeline for shoot ion accumulation in 100 mM NaCl, we selected
378 a 4-day time point for further experiments, as the differences in both Na^+ and Cl^- accumulation
379 in NIL-T and NIL-S tissues can be clearly discerned (Fig. 4, Fig. S5), and performed a more
380 detailed analysis of ion concentrations in a range of tissue types, and in the vascular sap. After
381 4 days, Na^+ accumulated to a greater extent in all aerial tissues in NIL-S, including leaves (both
382 first trifoliate leaf, FL, and youngest trifoliate leaf, YL), petioles of the first trifoliate leaf (FLP)
383 and youngest trifoliate leaf (YLP), higher stem (HS), lower stem (LS), and hypocotyl (Hy).
384 This is consistent with what we observed for whole shoot ion content analysis. No significant
385 differences were observed between the NILs for Na^+ in roots under salt treatment (primary root,
386 PR and secondary root, SR; Fig. 4a). Under control conditions (4 days), Na^+ content very low,
387 but significantly higher in secondary root (SR) of NIL-T compared to NIL-S, with no
388 significant differences in other tissues (Fig. S5). No significant differences between NIL-T and
389 NIL-S were observed for K^+ under control conditions (Fig. S5). And except for the higher K^+
390 accumulation in leaves, no differences were found in any other of the investigated aerial tissues
391 or roots (Fig. 4b).

392 Cl^- accumulation pattern showed similarities but also differences to that of Na^+
393 accumulation, under saline conditions. In aerial parts and hypocotyls more Cl^- accumulated in
394 leaves, stems and hypocotyls of NIL-S compared to NIL-T (Fig. 4c), similar to Na^+. While we

395 found that in roots (PR and SR), NIL-T accumulated significantly more Cl^- than NIL-S (Fig.
396 4c). Under control conditions, Cl^- content was significantly elevated in leaves and stem of NIL-
397 S, with no differences for hypocotyl and roots (Fig. S5). We also measured NO_3^- content and
398 found that NIL-S accumulated less NO_3^- in leaves (both FL and YL) and roots in compared to
399 NIL-T, which lead to a high. Cl^- to NO_3^- ratio in leaves of NIL-S, but not in roots (Fig. 4d). In
400 summary, significantly less Na^+, K^+, and Cl^- accumulated in NIL-T shoots than NIL-S under
401 saline conditions. Leaf ion exclusion is in many plant species achieved by retention of ions in
402 the root, primarily by reducing net ion concentration in the shoot-ward direction solute flow.
403 To investigate if this is also the case in soybean, we determined xylem and phloem sap ion
404 concentrations.

405 Ion concentrations within soybean stem phloem and xylem sap were examined at the
406 4-day time point following NaCl treatment. Glutamine contents within the phloem sap was
407 used to normalize ion measurements to account for volume differences measurements, as
408 glutamine concentration within the phloem remains constant throughout the day (Corbesier,
409 Havelange, Lejeune, Bernier, & Périlleux, 2001). It was found that our estimates of Na^+ and
410 K^+ contents were not significantly different between the phloem sap of NIL-T and -S plants.
411 As expected, the Na^+ concentration in the xylem sap in NIL-S was significantly greater
412 compared to NIL-T, indicating less Na^+ is loaded into the xylem, or more is retrieved.
413 Surprisingly, and in apparent contrast to the leaf accumulation data, the Cl^- concentration in
414 xylem sap was lower in NIL-S than NIL-T (Fig. 5b). In addition to the higher xylem sap
415 concentrations, Cl^- concentration was also significantly higher in the phloem sap in NIL-T (Fig.
416 5a). Phloem sap was harvested from a position where the flow direction is root-wards, close to
417 the junction of root and shoot. The higher Cl^- in NIL-T phloem sap therefore indicated an
418 increased flow of Cl^- from the shoot to the roots in NIL-T plants, this would be consistent with
419 Cl^- being recirculated from the stem to the roots via the phloem. Under control conditions (4
420 days with water treatment), no significant differences were observed between NIL-T and NIL-
421 S for the ion concentrations within stem phloem and xylem sap (Fig. S5d), which may be
422 related to the detection levels of the assays.

423 The observed higher Cl^- concentration in phloem sap suggested that the leaf Cl^-
424 exclusion mechanism in NIL-T might be derived from the shoot, instead of the root. To
425 investigate this, a grafting experiment was performed. Reciprocally grafted and self-grafted
426 control plants were salt-treated (100 mM NaCl) for 8 days, as previously described (Guan et
427 al., 2014). The differences in Na^+ that we observed were consistent with previous grafting

428 experiments, confirming that Na^+ exclusion depends on a root derived mechanism (Fig. S6a,
429 Guan et al., 2014). In contrast to the situation with Na^+, grafting demonstrated that the scion,
430 not the rootstock, is important for leaf Cl^- exclusion. When a NIL-T scion was grafted on a
431 NIL-S rootstock, the Cl^- content in leaves was 89.1% lower when compared to leaves of self-
432 grafted NIL-S (Fig. 6a); with fresh and dry weight calculations showing the same trend (Figure
433 6b). Conversely, when the NIL-S scion was grafted on the NIL-T rootstock, the Cl^- content in
434 leaves was not significantly different compared to self-grafted NIL-S (Fig. 6a). Controls
435 confirmed that self-grafted NIL-S had a considerably higher Cl^- content compared to self-
436 grafted NIL-T (Fig. 6a), as expected. In the roots, no significant difference were detected
437 between grafted plants (Fig. 6c).
438 As we identified the phloem as an important component of the GmSALT3-derived salt
439 exclusion mechanism, we investigated the ultrastructure of the phloem to identify possible
440 differences between NIL-T and NIL-S. In the phloem, the ER of companion cells reaches into
441 the sieve elements and is directly exposed to the phloem sap (Turgeon & Wolf, 2009). This
442 could theoretically enable a direct ion transport from and into the sap of phloem cells, through
443 the ER-localised GmSALT3, and/or loss of GmSALT3 could lead to morphological changes
444 of the ER ultrastructure. TEM (Transmission Electron Microscopy) imaging did not reveal
445 obvious morphological differences between salt-treated NIL-T and NIL-S in root phloem cells
446 (Fig. S7), indicating lack of full-length *GmSALT3* does not result in a disruption to sub-cellular
447 morphology and that changes in ion flux are more likely directly responsible.
448

449 **Discussion**

450 **Transport function of GmSALT3**

451 Plant CPA2 (Cation-Proton Antiporter 2)/CHX (Cation/H^+ Exchangers) have
452 traditionally been characterised using knockout strains of yeast. A close homolog of
453 GmSALT3, AtCHX20 in *Arabidopsis thaliana*, is preferentially expressed in stomatal guard
454 cells, and shows a localisation pattern consistent with ER-localisation, like GmSALT3
455 (Padmanaban et al., 2007). Similar to GmSALT3, expression of *AtCHX20* was shown to
456 enhance growth of (a different) *E. coli* strain deficient in K^+ uptake (LB2003) (Chanroj et al.,
457 2011), indicating that the two proteins catalyse the transport of K^+. This assay also showed that
458 YFP-tagged GmSALT3 and GmSALT3-TM10 were also functional for K^+ transport, but not
459 the truncated Gmsalt3, which lacks the last membrane embedded TM10. This suggests that the
460 entire set of transmembrane domains are required for ion transport, and that Gmsalt3 is non-

461 transport competent. Our results further suggest that the large C-terminus, found in all plant
462 CHX proteins, is not required for CHX to conduct ion transport.
463 We then attempted a transport assay with greater resolution i.e. *X. laevis* oocytes, which
464 has not been previously reported for plant CHX proteins. Using oocytes, two *Drosophila* CPA2
465 transporters, NHA1 and NHA2, were speculated to act as a Na^+/H^+ exchanger and a H^+/Cl^-
466 cotransporter, respectively (Chintapalli et al., 2015), indicating that proteins from this family
467 can putatively act as either, cation or anion transporters. We observed that GmSALT3 targeted
468 to the PM (Fig. 2a), unlike *in planta*, and led to a lower net ion efflux of all three ions (K^+, Na^+
469 and Cl^-) across the PM (Fig. 2c). Interestingly, the reduced efflux effect was inhibited by the
470 Na^+ channel and Na^+/H^+ exchanger inhibitor amiloride hydrochloride. Whilst this inhibitor is
471 thought to be selective for Na^+ transporters, it had an impact on the efflux rate of all three ions
472 measured. It is possible that observed differences in ion flux and accumulation in heterologous
473 systems are the result of changing cytosolic ion concentration that then impacts ion gradients
474 across the PM and influences the activity of native ion transporters. In such a scenario the
475 fluxes detected across the PM of oocytes would be the result of a combination of GmSALT3
476 and native transporters; and the inhibition of one component leads to the inhibition of the entire
477 mechanism. To conclusively characterise the transport properties of GmSALT3 alternative
478 techniques will need to be employed such as the incorporation of pure protein into liposomes
479 devoid of other transport proteins (Nagarajan et al. 2016).
480
481 **The effect of GmSALT3 on ion accumulation *in planta* following salt treatment**
482 Salt tolerance includes tolerance to elevated levels of both Cl^- and Na^+ in the soil
483 solution. In many plant species one of the two ions is understood to be more deleterious to the
484 plant when accumulated in the tissue; however, the situation for soybean is currently unclear
485 with evidence for both ions being more toxic than the other (Läuchli, 1984). Whilst our work
486 does not answer which ion is the most toxic, it does clearly demonstrate that Na^+ and Cl^- long
487 distance transport, and its accumulation in shoots, can be connected to a single gene, which
488 renders the tolerance mechanisms currently inseparable. That said, although leaf Na^+ and Cl^-
489 exclusion are connected to the same gene, *GmSALT3*, confers two distinct mechanisms that are
490 uncoupled *in planta*. Initial evidence suggested that two separate leaf ion exclusion
491 mechanisms exist in soybean comes from our experiments using plants treated with 100 mM
492 NaCl. This salt concentration mimics a more physiologically relevant salt treatment than has
493 previously been used on NIL plants (i.e. one that would be found in the field). Our data
494 suggested that in these conditions shoot exclusion of Cl^- broke down prior to exclusion of Na^+

495 in NIL-S when compared with NIL-S plants (Fig. 3), and therefore, the mechanisms regulating
496 Cl^- and Na^+ transport are likely to be distinct. More conclusive evidence was highlighted by
497 the reciprocal grafting of NIL-T and NIL-S shoots and roots. These data indicate GmSALT3
498 is likely to function in the shoot and stem to limit the accumulation of Cl^- in the shoot (Fig.
499 6a). In contrast, Na^+ was accumulated to greater concentrations in the aerial parts of NIL-S but
500 no difference was observed in the roots compared to NIL-T (Fig. 4a); in stem xylem sap, there
501 was a lower Na^+ concentration in NIL-T compared to NIL-S but no significant difference in
502 stem phloem sap estimations (Fig. 5). This indicates more Na^+ is transported in the NIL-S
503 xylem stream. Na^+ measurements in leaves, xylem sap and the grafting experiment are
504 consistent with a reduced net loading of Na^+ xylem in NIL-T roots. Root-derived Na^+ shoot
505 exclusion mechanisms are well known from other plant species, as described in the introduction.
506 Our new finding that shoot Cl^- exclusion is a phenotype conferred by the presence of
507 GmSALT3 in the shoots (through grafting) is consistent with our estimations of phloem Cl^-
508 content, and we propose is due to phloem recirculation of Cl^- back to the roots. Whilst phloem
509 retranslocation of NaCl in saline conditions has been observed before, where in maize
510 approximately 13-36% of the Na^+ and Cl^- imported to leaves through the xylem was
511 retranslocated to the root again in the phloem (Lohaus et al., 2000); no transport protein could
512 be linked to this phenomenon. Furthermore, phloem loading and unloading of Cl^- has not been
513 shown in any other plant species to efficiently correlate with salinity tolerance. The role of
514 GmSALT3 in the transfer of Cl^- from the xylem into the phloem sap is consistent with its
515 expression in vascular parenchyma cells in the root and shoot (Guan et al., 2014). Further
516 investigation is needed to increase our knowledge on this new tolerance mechanism and the
517 interconnection between xylem and phloem loading for Cl^- transport. The prevention of leaf
518 Cl^- accumulation, together with the higher NO_3^- content, suggest that NIL-T may maintain
519 increased metabolic and photosynthetic activity in shoots by maintaining a low Cl^-/NO_3^- ratio,
520 while NIL-S might suffer from Cl^- toxicity (Li et al., 2017; Wege, Gilliham & Henderson,
521 2017).
522
523 **Putative *in planta* mechanisms for GmSALT3 regulating long distance ion transport**
524 Coupled to the complexities of identifying the transport properties of GmSALT3 in its
525 native membrane (the endoplasmic reticulum (Guan et al., 2014), and the complex and distinct
526 processes underlying the different salt ion accumulation phenotypes of the two NILs, we
527 propose that GmSALT3 affects processes at the ER and is not directly mediating ion transport
528 across the PM or tonoplast itself – this makes it unlike most other transport proteins identified

529 as important for salt tolerance. Instead, we propose that, *in planta*, the endomembrane localised
530 GmSALT3 influences ion gradients across the PM through currently unknown downstream
531 effects. This might be through impacting the activity of PM-localised transporters, by changing
532 their PM-abundance or changing cytosolic ion supply, or even more complex effects. For
533 example, if the ionic milieu within the ER is affected this could impact the function or sorting
534 of other membrane transporters or regulatory proteins (Bayer et al., 2017), which then impacts
535 PM fluxes; similarly, a difference in the ER-membrane potential could lead to such effects.
536 How GmSALT3 differentially affects the long-distance transport pathways in shoots and roots
537 will now need to be prioritised. Further experiments will need to be carried out to decipher the
538 novel mechanisms imparted by GmSALT3 that are important for salt tolerance. This might
539 enable us to identify similar mechanisms in other (crop) plants.
540

541 **Conclusion**

542 To summarize, this work has provided further insights into the salinity tolerance
543 mechanisms imparted by GmSALT3 *in planta* and in heterologous systems. We propose that,
544 in NIL-T, the presence of full-length *GmSALT3* mediates Na^+ and Cl^- exclusion from shoots
545 through restricting net xylem loading of Na^+, while Cl^- is retranslocated from the shoots back
546 into the roots via the phloem. This is the first time that a protein has been shown to confer
547 phloem recirculation of Cl^-, and that this confers trait improved salt tolerance *in planta*. Our
548 data also demonstrates that GmSALT3 is a transport competent endomembrane localised
549 protein, but fall short of describing the exact cellular mechanisms through which GmSALT3
550 alters differential transport processes across different cell-types, which is an area that requires
551 further study. RNA-sequencing using NIL-T and NIL-S plants may be beneficial in
552 investigating if GmSALT3 confers salinity tolerance in soybean via influencing transcription,
553 and what distinctive pathways and genes might be significantly changed in NIL-T and NIL-S
554 roots under saline conditions.
555

556 **Acknowledgements**

557 We thank Dr. Yue (Crystal) Wu for generating the *AtCBL1n* entry vector; Sunita
558 Ramesh and Zhonghua Chen for providing *AtKAT1* construct used in this study; CSIRO,
559 Australia for donating *E. coli* strain TK2463. We thank Adelaide Microscopy, especially
560 Gwenda Mayo for the use of TEM and other imaging facilities. This work was funded by the
561 Natural Science Foundation of China, grant number 31830066 (RG). YQ and SH were

supported by ARC Centre of Excellence funding awarded to MG (CE140100008). ARC Fellowships supported MG (FT130100709), SW (DE160100804) and JB (DE170100346).

Author contributions

MG, YQ and SW designed experiments, with input from LQ and RG. LQ and MG directed the project. YQ performed ion accumulation measurement, TEM, IRGA, *E. coli* and oocyte expression, analysed the data and drafted the manuscript. JB performed MIFE in oocytes. SH assisted with experimental design and provided the *E. coli* expression vectors. YQ, MG and SW wrote the manuscript. All authors commented on the manuscript.

References

Abel G. (1969). Inheritance of the capacity for chloride inclusion and chloride exclusion by soybeans. *Crop Science*, 9, 697-698.

Alexandratos N. & Bruinsma J. (2012). World agriculture towards 2030/2050: the 2012 revision: ESA Working paper No.12-03. Rome, FAO.

Anderson J.A., Huprikar S.S., Kochian L.V., Lucas W.J. & Gaber R.F. (1992). Functional expression of a probable *Arabidopsis thaliana* potassium channel in *Saccharomyces cerevisiae*. *Proceedings of the National Academy of Sciences*, 89, 3736-3740.

Batistič O., Waadt R., Steinhorst L., Held K. & Kudla J. (2010). CBL-mediated targeting of CIPKs facilitates the decoding of calcium signals emanating from distinct cellular stores. *The Plant Journal*, 61, 211-222.

Bayer E.M., Sparkes I., Vanneste S. & Rosado A. (2017). From shaping organelles to signalling platforms: the emerging functions of plant ER–PM contact sites. *Current Opinion in Plant Biology* 40, 89–96.

Berthomieu P., Conéjéro G., Nublat A., Brackenbury W.J., Lambert C., Savio C., Uozumi N., Oiki S., Yamada K. & Cellier F. (2003). Functional analysis of AtHKT1 in Arabidopsis shows that Na^+ recirculation by the phloem is crucial for salt tolerance. *The EMBO Journal*, 22, 2004-2014.

Blanco, F.F., M.V. Folegatti, H.R. Gheyi, and P.D. Fernandes. 2007. Emergence and growth of corn and soybean under saline stress. *Scientia Agricola*. 64:451–459.

Cao D., Li Y., Liu B., Kong F., & Tran L.S.P. (2018). Adaptive mechanisms of soybean grown on salt-affected soils. *Land Degradation & Development*, 29, 1054-1064.

Chang R.Z., Chen Y.W., Shao G.H., Wan C.W. (1994). Effect of salt stress on agronomic characters and chemical quality of seeds in soybean. *Soybean Science*, 13, 101-105.

Chanroj S., Lu Y., Padmanaban S., Nanatani K., Uozumi N., Rao R. & Sze H. (2011). Plant-specific cation/H^+ exchanger 17 and its homologs are endomembrane K^+ transporters with roles in protein sorting. *Journal of Biological Chemistry*, 286, 33931-33941.

Chintapalli V.R., Kato A., Henderson L., Hirata T., Woods D.J., Overend G., Davies S.A., Romero M.F. & Dow J.A. (2015). Transport proteins NHA1 and NHA2 are essential for survival, but have distinct transport modalities. *Proceedings of the National Academy of Sciences*, 112, 11720-11725.

602 Corbesier L., Havelange A., Lejeune P., Bernier G. & Périlleux C. (2001). N content of phloem
603 and xylem exudates during the transition to flowering in *Sinapis alba* and *Arabidopsis*
604 *thaliana*. *Plant, Cell & Environment*, 24, 367-375.
605 Czerny D.D., Padmanaban S., Anishkin A., Venema K., Riaz Z. & Sze H. (2016). Protein
606 architecture and core residues in unwound α-helices provide insights to the function of
607 a plant transporter AtCHX17. *Biochimica et Biophysica Acta (BBA)-Biomembranes,*
608 1858, 1983-1998.
609 Darley, C.P., Van Wuytswinkel, O.C., Van der woude, K. and Mager, W.H. (2000).
610 Arabidopsis thaliana and Saccharomyces cerevisiae NHX1 genes encode amiloride
611 sensitive electroneutral Na^+/H^+ exchangers. *Biochemical Journal*, 351, 241-249.
612 Do T.D., Chen H., Hien V.T.T., Hamwieh A., Yamada T., Sato T., Yan Y., Cong H., Shono
613 M. & Suenaga K. (2016). Ncl synchronously regulates Na^+, K^+, and Cl^- in soybean and
614 greatly increases the grain yield in saline field conditions. *Scientific Reports*, 6, 19147.
615 Epstein W., Buurman E., McLaggan D. & Naprstek J. (1993). Multiple mechanisms, roles and
616 controls of K^+ transport in *Escherichia coli*: Portland Press Limited.
617 FAO. (2017). *The future of food and agriculture – Trends and challenges*, Rome: FAO.
618 Gilliham M., Able J.A. & Roy S.J. (2017). Translating knowledge about abiotic stress tolerance
619 to breeding programmes. *The Plant Journal*. 90, 898-917.
620 Guan R., Qu Y., Guo Y., Yu L., Liu Y., Jiang J., Chen J., Ren Y., Liu G. & Tian L. (2014).
621 Salinity tolerance in soybean is modulated by natural variation in *GmSALT3*. *The Plant*
622 *Journal*, 80, 937-950.
623 Guo J., Zhou Q., Li X., Yu B. & Luo Q. (2017). Enhancing NO_3^- supply confers NaCl tolerance
624 by adjusting Cl^- uptake and transport in *G. max* & *G. soja*. *Journal of Soil Science and*
625 *Plant Nutrition*, 17, 194-202.
626 Ha B.K., Vuong T.D., Velusamy V., Nguyen H.T., Shannon J.G. & Lee J.D. (2013). Genetic
627 mapping of quantitative trait loci conditioning salt tolerance in wild soybean (*Glycine*
628 *soja*) PI 483463. *Euphytica*. 193, 79-88.
629 Hamwieh A., Tuyen D.D., Cong H., Benitez E.R., Takahashi R. & Xu, D.H. (2011).
630 Identification and validation of a major QTL for salt tolerance in soybean. *Euphytica,*
631 179, 451-459.
632 Hamwieh A. & Xu D. (2008). Conserved salt tolerance quantitative trait locus QTL) in wild
633 and cultivated soybeans. *Breeding Science*, 58, 355-359.
634 Ikeda M. (2005). Distribution of K^+, Na^+ and Cl^- in root and leaf cells of soybean and cucumber
635 plants grown under salinity conditions. *Soil Science and Plant Nutrition*, 51, 1053-1057.

636 Lee G.J., Carter J.T.E., Villagarcia M.R., Li Z., Zhou X., Gibbs M.O. & Boerma H.R. (2004).
637 A major QTL conditioning salt tolerance in S-100 soybean and descendent cultivars.
638 *Theoretical and Applied Genetics*, 109, 1610-1619.
639 Lenis J., Ellersieck M., Blevins D., Sleper D., Nguyen H., Dunn D., Lee J. & Shannon J. (2011).
640 Differences in ion accumulation and salt tolerance among *Glycine* accessions. *Journal*
641 *of Agronomy and Crop Science*. 197, 302-310.
642 Li B., Tester M. & Gilliham M. (2017). Chloride on the Move. *Trends in Plant Science*, 22,
643 236-248.
644 Li W.Y., Wong F.L., Tsai S.N., Phang T.H., Shao G. & Lam H.M. (2006a). Tonoplast-located
645 *GmCLC1* and *GmNHX1* from soybean enhance NaCl tolerance in transgenic bright
646 yellow (BY)-2 cells. *Plant Cell & Environment*, 29, 1122-1137.
647 Li X.J., An P., Inanaga S., Eneji A.E. & Tanabe K. (2006b). Salinity and defoliation effects on
648 soybean growth. *Journal of Plant Nutrition*, 29, 1499-1508.
649 Liu Y., Yu L., Qu Y., Chen J., Liu X., Hong H., Liu Z., Chang R., Gilliham M., Qiu L. & Guan
650 R. (2016). GmSALT3, which confers improved soybean salt tolerance in the field,
651 increases leaf Cl^- exclusion prior to Na^+ exclusion but does not improve early vigor
652 under salinity. *Frontiers in Plant Science*, 7, 1485
653 Lohaus G., Hussmann M., Pennewiss K., Schneider H., Zhu J.J. & Sattelmacher B. (2000).
654 Solute balance of a maize (*Zea mays* L.) source leaf as affected by salt treatment with
655 special emphasis on phloem retranslocation and ion leaching. *Journal of Experimental*
656 *Botany*, 51, 1721-1732.
657 Luo G.Z., Wang H.W., Huang J., Tian A.G., Wang Y.J., Zhang J.S. & Chen S.Y. (2005a). A
658 putative plasma membrane cation/proton antiporter from soybean confers salt tolerance
659 in Arabidopsis. *Plant Molecular Biology*, 59, 809-820.
660 Luo Q., Yu B. & Liu Y. (2005b). Differential sensitivity to chloride and sodium ions in
661 seedlings of *Glycine max* and *G. soja* under NaCl stress. *Journal of Plant Physiology*,
662 162, 1003-1012.
663 Läuchli A. (1984). Salt exclusion: An adaptation of legumes for crops and pastures under saline
664 conditions. In *Salinity Tolerance in Plants: Strategies for Crop Improvement* (Staples,
665 R.C. and Toenniessen, G.H. eds). New York: Wiley, pp. 171-187.
666 Masrati G., Dwivedi M., Rimon A., Gluck-Margolin Y., Kessel A., Ashkenazy H., Mayrose I.,
667 Padan E. and Ben-Tal N. (2018). Broad phylogenetic analysis of cation/proton
668 antiporters reveals transport determinants. *Nature communications*, 9, 4205.

669 Maurel C., Reizer J., Schroeder J.I. & Chrispeels M.J.. (1993). The vacuolar membrane protein
670 gamma-TIP creates water specific channels in *Xenopus oocytes*. *The EMBO Journal*,
671 12, 2241-2247.
672 Munns R., Day D.A., Fricke W., Watt M., Arsova B., Barkla B.J., Bose J., Byrt C.S., Chen Z.-
673 H., Foster K.J., Gilliham M., Henderson S.W., Jenkins C.L.D., Kronzucker H.J.,
674 Miklavcic S.J., Plett D., Roy S.J., Shabala S., Shelden M.C., Soole K.L., Taylor N.L.,
675 Tester M., Wege S., Wegner L.H. and Tyerman S.D. (2020), Energy costs of salt
676 tolerance in crop plants. *New Phytologist*, 225, 1072-1090.
677 Munns R. & Gilliham M. (2015). Salinity tolerance of crops–what is the cost? *New Phytologist*,
678 208, 668-673.
679 Munns R., James R.A., Xu B., Athman A., Conn S.J., Jordans C., Byrt C.S., Hare R.A.,
680 Tyerman S.D. & Tester M. (2012). Wheat grain yield on saline soils is improved by an
681 ancestral Na^+ transporter gene. *Nature Biotechnology*, 30, 360-364.
682 Møller I.S., Gilliham M., Jha D., Mayo G.M., Roy S.J., Coates J.C., Haseloff J. & Tester M.
683 (2009). Shoot Na^+ exclusion and increased salinity tolerance engineered by cell type-
684 specific alteration of Na^+ transport in *Arabidopsis*. *Plant Cell*, 21, 2163-2178.
685 Nagarajan Y., Rongala, J., Luang S., Singh A., Shadiac N., Hayes J., Sutton T., Gilliham M.,
686 Tyerman S.D., McPhee G., Voelcker N.H., Mertens H.D.T., Kirby N.M., Lee J.-G.,
687 Yingling Y.G., Hrmova M., 2016. A barley efflux transporter operates in a Na^+-
688 dependent manner, as revealed by a multidisciplinary platform. *Plant Cell* 28, 202-218.
689 Newman, I. (2001). Ion transport in roots: measurement of fluxes using ion-selective
690 microelectrodes to characterize transporter function. *Plant, Cell & Environment* 24**,** 1-
691 14.
692 Obermeyer G. & Tyerman S.D. (2005). NH_4^+ currents across the peribacteroid membrane of
693 soybean. Macroscopic and microscopic properties, inhibition by Mg^{2+}, and temperature
694 dependence indicate a SubpicoSiemens channel finely regulated by divalent cations.
695 *Plant Physiology*, 139, 1015-1029.
696 Padmanaban S., Chanroj S., Kwak J.M., Li X., Ward J.M. & Sze H. (2007). Participation of
697 endomembrane cation/H^+ exchanger *AtCHX20* in osmoregulation of guard cells. *Plant*
698 *Physiology*, 144, 82-93.
699 Phang T.H., Shao G. & Lam H.M. (2008). Salt tolerance in soybean. *Journal of Integrative*
700 *Plant Biology*, 50, 1196-1212.

701 Phang T.H., Shao G., Liao H., Yan X. & Lam H.M. (2009). High external phosphate (Pi)
702 increases sodium ion uptake and reduces salt tolerance of 'Pi-tolerant'soybean.
703 *Physiologia Plantarum*, 135, 412-425.
704 Qi X., Li M.W., Xie M., Liu X., Ni M., Shao G., Song C., Yim A.K.Y., Tao Y., Wong F.L. &
705 Isobe S. (2014). Identification of a novel salt tolerance gene in wild soybean by whole-
706 genome sequencing. *Nature Communications*, 5, 4340.
707 Qiu J., Henderson S.W., Tester M., Roy S.J. & Gilliham M. (2016). SLAH1, a homologue of
708 the slow type anion channel SLAC1, modulates shoot Cl^- accumulation and salt
709 tolerance in *Arabidopsis thaliana*. *Journal of Experimental Botany*, 67, 4495-4505.
710 Ren Z.H., Gao J.P., Li L.G., Cai X.L., Huang W., Chao D.Y., Zhu M.Z., Wang Z.Y., Luan S.
711 & Lin H.X. (2005). A rice quantitative trait locus for salt tolerance encodes a sodium
712 transporter. *Nature Genetics*, 37, 1141-1146.
713 Roy S.J., Negrão S. & Tester M. (2014). Salt resistant crop plants. *Current Opinion in*
714 *Biotechnology*, 26, 115-124.
715 Rupassara S.I. (2008). Metabolite profiling of leaves and vascular exudates in soybean grown
716 under free-air concentration enrichment. PhD thesis, University of Illinois at Urbana-
717 Champaign.
718 Rus A., Baxter I., Muthukumar B., Gustin J., Lahner B., Yakubova E. & Salt D.E. (2006).
719 Natural variants of AtHKT1 enhance Na^+ accumulation in two wild populations of
720 *Arabidopsis*. *PLoS Genetics*, 2, 210.
721 Shabala S., Shabala L., Bose J., Cuin T. & Newman I. (2013). Ion flux measurements using
722 the MIFE technique. *Plant Mineral Nutrients: Methods and Protocols*, 171-183.
723 Shi H., Bressan R. (2006). RNA extraction. *Methods in Molecular Biology* 323: 345.
724 Singh G. (2010). *The soybean: botany, production and uses.* Oxfordshire, UK: CABI
725 Publishing.
726 Sze H. & Chanroj S. (2018). Plant endomembrane dynamics: Studies of K^+/H^+ antiporters
727 provide insights on the effects of pH and ion homeostasis. *Plant Physiology*, 177, 875-
728 95.
729 Tester M. & Davenport R. (2003). Na^+ tolerance and Na^+ transport in higher plants. *Annals of*
730 *Botany*, 91, 503-527.
731 Tester M. & Langridge P. (2010). Breeding technologies to increase crop production in a
732 changing world. *Science*, 327, 818-822.

733 Tian H., Baxter I.R., Lahner B., Reinders A., Salt D.E. & Ward J.M. (2010). Arabidopsis
734 NPCC6/NaKR1 is a phloem mobile metal binding protein necessary for phloem
735 function and root meristem maintenance. *The Plant Cell*, 22, 3963-3979.
736 Turgeon R. & Wolf S. (2009). Phloem transport: cellular pathways and molecular trafficking.
737 *Annual Review of Plant Biol*ogy, 60, 207-221.
738 Uozumi N., Kim E.J., Rubio F., Yamaguchi T., Muto S., Tsuboi A., Bakker E.P., Nakamura T.
739 & Schroeder J.I. (2000). The Arabidopsis *HKT1* gene homolog mediates inward Na^+
740 currents in *Xenopus laevis* oocytes and Na^+ uptake in *Saccharomyces cerevisiae*. *Plant*
741 *Physiology,* 122, 1249-1260.
742 Wege S., Gilliham M. & Henderson, S.W. (2017). Chloride: not simply a 'cheap osmoticum',
743 but a beneficial plant macronutrient. *Journal of Experimental Botany*, 68, 3057-3069.
744 Xu G.H., Magen H., Tarchitzky J. & Kafkafi U. (2000). Advances in chloride nutrition of
745 plants. San Diego: Academic Press Inc., pp. 97-150.
746

747 **Figure Legends**

748 **Figure 1 Functional test of *GmSALT3* in *E. coli*.** *E. coli* strain TK2463 (defective in
749 potassium uptake, Trk, Kup, and Kdp) harbouring a modified pET-DEST42 vector with
750 *GmSALT3, Gmsalt3, CBL1n, GmSALT3-YFP, GmSALT3-TM10, AtCHX20 and AtKAT1* were
751 grown in different media. (**a**) Low potassium medium (10 g/L tryptone, 2 g/L yeast extract,
752 100 mM D-mannitol; ~2 mM K^+) with additional 0.5 mM Isopropyl β- D-1-
753 thiogalactopyranoside (IPTG). All the test media were supplemented with 100 µg/ml
754 carbenicillin. OD_{600} was monitored every 15 min in 96-well microplate reader. n = 3. Growth
755 rates (OD_{600} per hour) of *E. coli* cells within the log phase are indicated between dotted lines,
756 and their slopes are shown in (**b**) (low potassium medium with IPTG). Different letters indicate
757 statistically significant differences between *E. coli* cells harbouring different constructs (one-
758 way ANOVA followed by Fisher's LSD test, $p < 0.05$).

759

760 **Figure 2 Functional characterization of *GmSALT3* in *X. laevis* oocytes. (a)** Plasma
761 membrane localisation of expressed *GmSALT3-YFP* in oocytes. H_2O-injected and *TmHKT1;5-*
762 *A*-YFP (positive control) expressed oocytes are also shown. Scale bar = 0.5 mm. Oocytes were
763 analysed by confocal laser-scanning microscopy. (**b**) Resting membrane potentials of
764 *GmSALT3*- and H_2O-injected oocytes after incubation in ND96 for 72 hours. n = 8, Asterisks
765 indicate a significant difference between GmSALT3- and H_2O-injected oocytes at $*p < 0.01$
766 according to the LSD test. (**c**) Net ion fluxes were measured on oocytes plasma membrane
767 using MIFE (Microelectrode Ion Flux Estimation). Oocytes were incubated in ND96 for 72
768 hours, and washed in ND96 in (96 mM NaCl, 1 mM KCl, 1 mM $MgCl_2$, 5 mM HEPES, pH
769 7.5). Measurements were done in BSM (Basal Salt Medium; 5 mM NaCl, 0.2 mM KCl, 0.2
770 mM $CaCl_2$, 5 mM HEPES, pH 7.5) and exchanged after time zero to BSM with sufficiently
771 low concentrations of Na^+, K^+ and Cl^- to ensure a gradient for efflux for target ions and an
772 improved signal:noise ratio. n = 4 - 6. (**d**) Ion (Na^+, K^+, and Cl^-) concentrations in *GmSALT3*
773 (black) and H_2O (grey) injected oocytes after incubation in ND96 (72 hours), BSM (overnight),
774 BSM with 100 µM amiloride (overnight). n = 4-7. Asterisks indicate a significant difference
775 between *GmSALT3*-injected and H_2O-injected oocytes at $*p < 0.05$, $**p < 0.01$ according to the
776 LSD test.

777

778 **Figure 3 Time-course ion concentration (mg DW^{-1}) in NIL-T and NIL-S leaves during 10**
779 **days 100 mmol L^{-1} NaCl stress.** Na^+ content (**a**), Cl^- content (**b**), K^+ (**c**) content, and K^+ to
780 Na^+ ratio (**d**) in leaves of NIL-T (black) and NIL-S (grey). Dry weight of different tissues (**e**;

comparisons are made between different tissues of NIL-T and NIL-S at different time points) and all tissues (**f**). n = 4. Asterisks indicates a significant difference between NIL-T and NIL-S at *p <0.05, **p < 0.01 according to the LSD test. DW, dry weight.

Figure 4 Ion concentration in different tissues of NIL-T and -S after 4 days of 100 mmol L^{-1} NaCl treatment. (**a**) Tissue content of Na^+ in leaf, hypocotyl and root of NILs. (**b**) K^+ content in leaf, hypocotyl and root of NILs. (**c**) Cl^- content in leaf, hypocotyl and root of NILs. (**d**) NO^{3-} content, Cl^- content and Cl^-/NO^{3-} ratio in leaf and root of NILs. Ion contents are expressed as tissue dry weight. n = 3-5. Asterisks indicate a significant difference between NIL-T (black) and NIL-S (grey) at *p <0.05, **p < 0.01 according to the LSD test (ion content data in control plants with water supply can be found in Figure S4). FL, first trifoliate leaves; YL, youngest trifoliate leaves; FLP, first trifoliate leaves petiole; YLP, youngest trifoliate leaves petiole; HS, higher stem; LS, lower stem; PR, primary root; SR, secondary root; Hy, hypocotyl. Data shown in (**a**), (**b**), and (**c**) were from one of the two independent experiments with similar results. Data shown in (**d**) were from a separate experiment and repeated twice.

Figure 5 Ion concentration in NIL-T and -S stem phloem and xylem sap after 4 days of 100 mmol L^{-1} NaCl stress. (**a**) Na^+, K^+, or Cl^- content to glutamine ratio in NIL-T and NIL-S stem phloem sap. (**b**) Na^+, K^+, and Cl^- concentrations in NIL-T (black) and NIL-S (grey) stem xylem sap. n = 3. Asterisks indicate a significant difference between NIL 820-T and 820-S at *p <0.05, **p < 0.01 according to the LSD test. SPS, stem phloem sap; SXS, stem xylem sap. Data shown here were from one of the three independent experiments with similar results.

Figure 6 Ion content (Cl^-) measurement of grafted NIL-T and NIL-S. The leaf Cl^- content **(a)** and Cl^- concentration **(b)** of reciprocally grafted and self-grafted NIL-T and NIL-S was measured under salt stress (100 mM NaCl) for 8 days. The root Cl^- content **(c)** was measured under same conditions. n = 6-11. Asterisks indicate a significant difference between NIL 820-T and 820-S at *p <0.05, **p < 0.01 according to the LSD test. T, NIL-T (*GmSALT3*); S, NIL-S (*Gmsal3*); ns, no significant difference.

815 **Supporting Information**

816 **Fig. S1. Functional test of *GmSALT3* in *E. coli* with low potassium and KML medium**.

817 **Fig. S2. Time-course ion concentration (Na^+) in NIL 820-T and 820-S leaves, stems,**
818 **hypocotyls, and roots during 10 days NaCl stress.**

819 **Fig. S3. Time-course ion concentration (K^+) in NIL 820-T and 820-S leaves, stems,**
820 **hypocotyls, and roots during 10 days NaCl stress.**

821 **Fig. S4. Time-course ion concentration (Cl^-) in NIL 820-T and 820-S leaves, stems,**
822 **hypocotyls, and roots during 10 days NaCl stress.**

823 **Fig. S5. Ion content and ion flux in NIL 820-T and 820-S different tissues after 4 days in**
824 **control conditions.**

825 **Fig. S6 Ion content (Na^+ and K^+) measurement of grafted NIL-T and NIL-S.**

826 **Fig. S7. Ultrastructure of NIL-*GmSALT3* and NIL-*Gmsalt3* root cross sections with 4 days**
827 **NaCl stress.**

828 **Table S1. Primers used in this study. Primers were designed and adjusted using Primer3.**

829

830

831

832

833 **Figures**

834

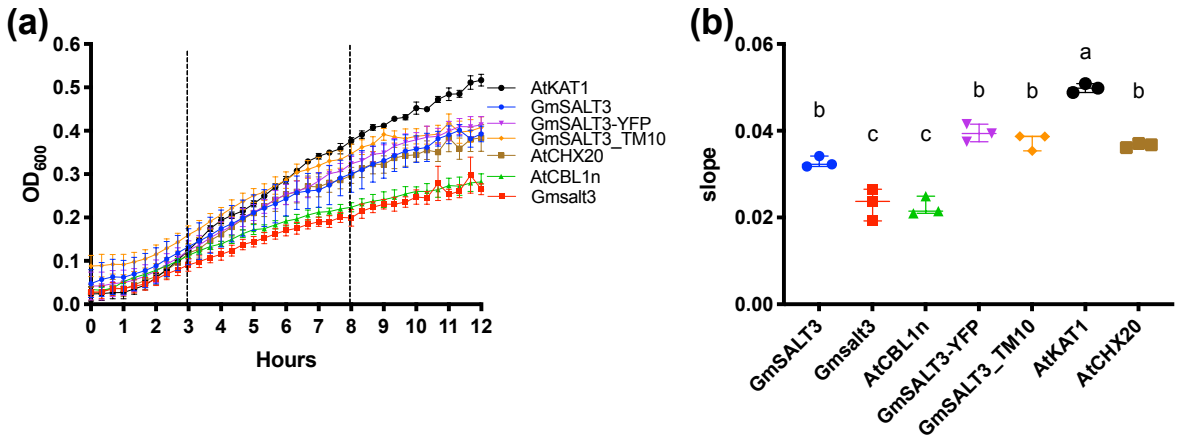

835

836 **Figure 1 Functional test of *GmSALT3* in *E. coli*.** *E. coli* strain TK2463 (defective in
837 potassium uptake, Trk, Kup, and Kdp) harbouring a modified pET-DEST42 vector with
838 *GmSALT3, Gmsalt3, CBL1n, GmSALT3-YFP, GmSALT3-TM10, AtCHX20 and AtKAT1* were
839 grown in different media. (**a**) Low potassium medium (10 g/L tryptone, 2 g/L yeast extract,
840 100 mM D-mannitol; ~2 mM K^+) with additional 0.5 mM Isopropyl β- D-1-
841 thiogalactopyranoside (IPTG). All the test media were supplemented with 100 µg/ml
842 carbenicillin. OD_{600} was monitored every 15 min in 96-well microplate reader. n = 3. Growth
843 rates (OD_{600} per hour) of *E.coli* cells within the log phase are indicated between dotted lines,
844 and their slopes are shown in (**b**) (low potassium medium with IPTG). Different letters indicate
845 statistically significant differences between *E. coli* cells harbouring different constructs (one-
846 way ANOVA followed by Fisher's LSD test, $p < 0.05$).

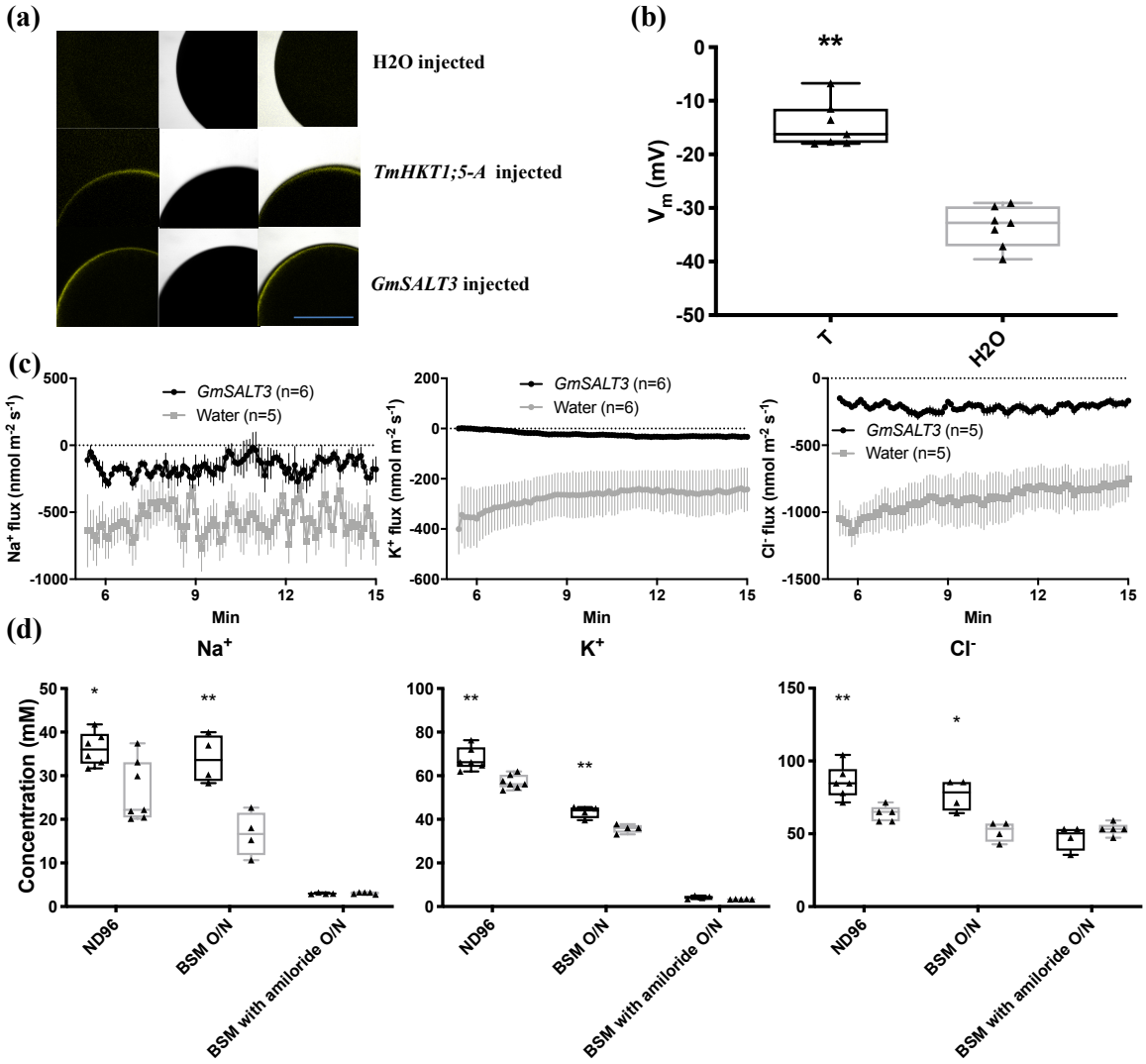

Figure 2 Functional characterization of *GmSALT3* in *X. laevis* oocytes. (a) Plasma membrane localisation of expressed *GmSALT3-YFP* in oocytes. H_2O-injected and *TmHKT1;5-A*-YFP (positive control) expressed oocytes are also shown. Scale bar = 0.5 mm. Oocytes were analysed by confocal laser-scanning microscopy. **(b)** Resting membrane potentials of *GmSALT3*- and H_2O-injected oocytes after incubation in ND96 for 72 hours. n = 8, Asterisks indicate a significant difference between GmSALT3- and H_2O-injected oocytes at $*p < 0.01$ according to the LSD test. **(c)** Net ion fluxes were measured on oocytes plasma membrane using MIFE (Microelectrode Ion Flux Estimation). Oocytes were incubated in ND96 for 72 hours, and washed in ND96 in (96 mM NaCl, 1 mM KCl, 1 mM $MgCl_2$, 5 mM HEPES, pH 7.5). Measurements were done in BSM (Basal Salt Medium; 5 mM NaCl, 0.2 mM KCl, 0.2 mM $CaCl_2$, 5 mM HEPES, pH 7.5) and exchanged after time zero to BSM with sufficiently low concentrations of Na^+, K^+ and Cl^- to ensure a gradient for efflux for target ions and an improved signal:noise ratio. n = 4 - 6. **(d)** Ion (Na^+, K^+, and Cl^-) concentrations in *GmSALT3*

861 (black) and H_2O (grey) injected oocytes after incubation in ND96 (72 hours), BSM (overnight),
862 BSM with 100 µM amiloride (overnight). n = 4-7. Asterisks indicate a significant difference
863 between *GmSALT3*-injected and H_2O-injected oocytes at $*p < 0.05$, $**p < 0.01$ according to the
864 LSD test.
865
866
867
868
869
870
871
872
873
874

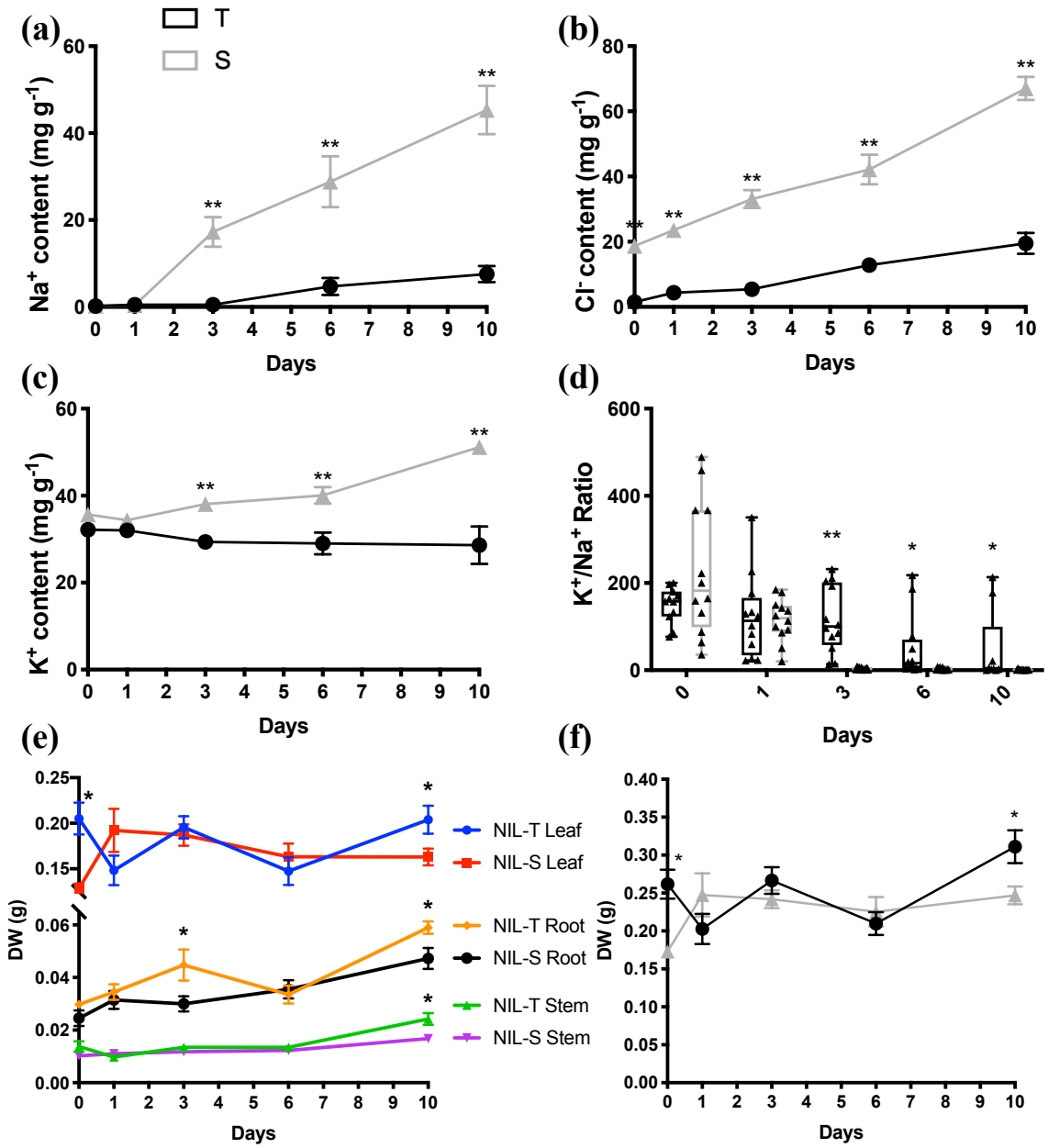

875

876 **Figure 3 Time-course ion concentration (mg DW^{-1}) in NIL-T and NIL-S leaves during 10**
877 **days 100 mmol L^{-1} NaCl stress.** Na^+ content (**a**), Cl^- content (**b**), K^+ (**c**) content, and K^+ to
878 Na^+ ratio (**d**) in leaves of NIL-T (black) and NIL-S (grey). Dry weight of different tissues (**e**;
879 comparisons are made between different tissues of NIL-T and NIL-S at different time points)
880 and all tissues (**f**). n = 4. Asterisks indicates a significant difference between NIL-T and NIL-
881 S at *p <0.05, **p < 0.01 according to the LSD test. DW, dry weight.

882

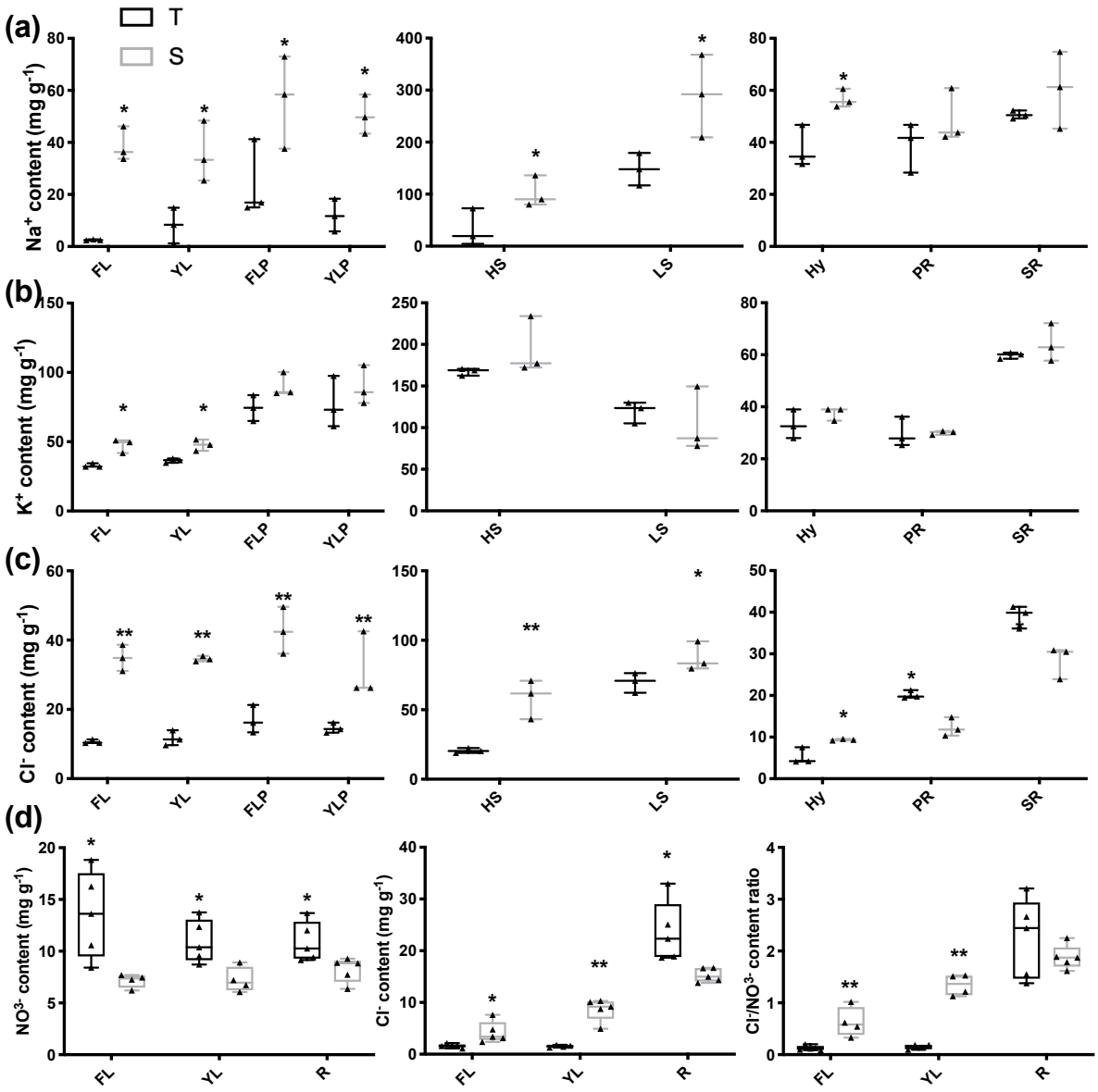

Figure 4 Ion concentration in different tissues of NIL-T and -S after 4 days of 100 mmol L^{-1} NaCl treatment. (**a**) Tissue content of Na^+ in leaf, hypocotyl and root of NILs. (**b**) K^+ content in leaf, hypocotyl and root of NILs. (**c**) Cl^- content in leaf, hypocotyl and root of NILs. (**d**) NO^{3-} content, Cl^- content and Cl^-/NO^{3-} ratio in leaf and root of NILs. Ion contents are expressed as tissue dry weight. n = 3-5. Asterisks indicate a significant difference between NIL-T (black) and NIL-S (grey) at $*p < 0.05$, $**p < 0.01$ according to the LSD test (ion content data in control plants with water supply can be found in Figure S4). FL, first trifoliate leaves; YL, youngest trifoliate leaves; FLP, first trifoliate leaves petiole; YLP, youngest trifoliate leaves petiole; HS, higher stem; LS, lower stem; PR, primary root; SR, secondary root; Hy, hypocotyl. Data shown in (**a**), (**b**), and (**c**) were from one of the two independent experiments with similar results. Data shown in (**d**) were from a separate experiment and repeated twice.

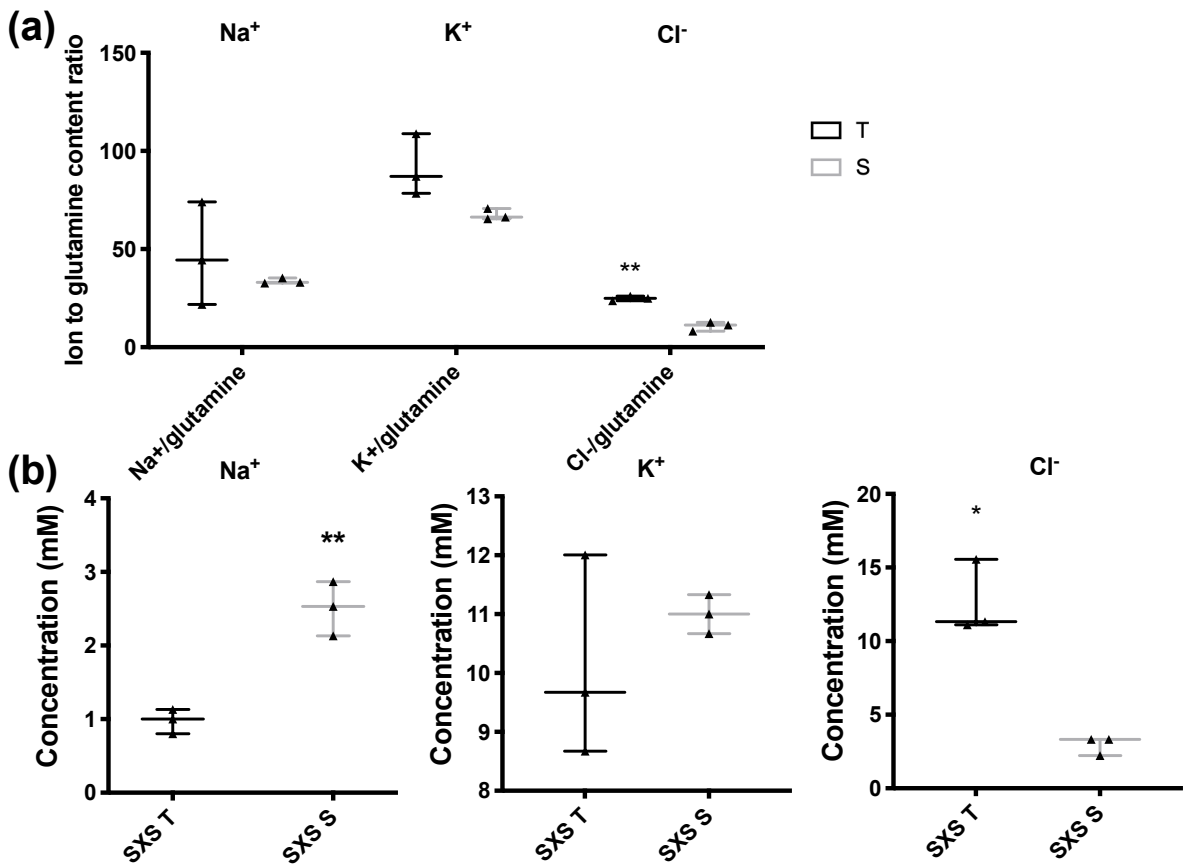

Figure 5 Ion concentration in NIL-T and -S stem phloem and xylem sap after 4 days of 100 mmol L^{-1} NaCl stress. (**a**) Na^+, K^+, or Cl^- content to glutamine ratio in NIL-T and NIL-S stem phloem sap. (**b**) Na^+, K^+, and Cl^- concentrations in NIL-T (black) and NIL-S (grey) stem xylem sap. n = 3. Asterisks indicate a significant difference between NIL 820-T and 820-S at *p <0.05, **p < 0.01 according to the LSD test. SPS, stem phloem sap; SXS, stem xylem sap. Data shown here were from one of the three independent experiments with similar results.

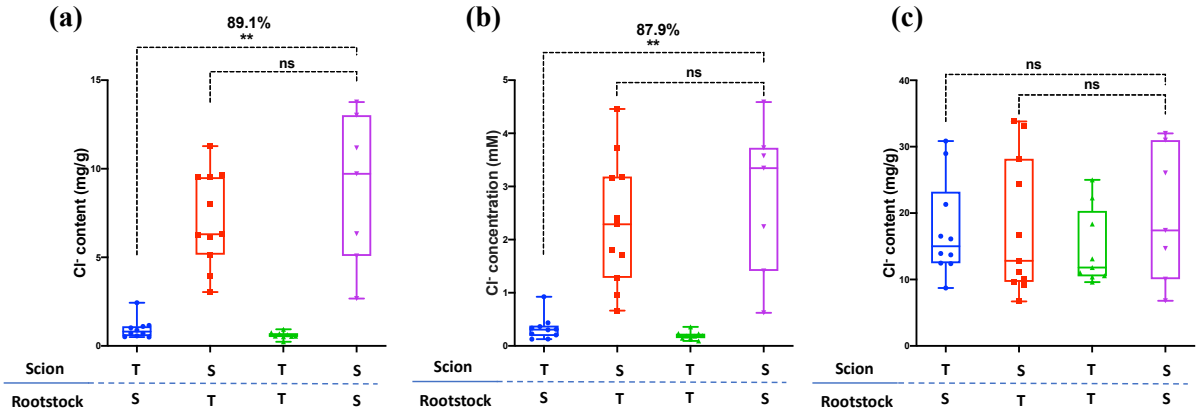

Figure 6 Ion content (Cl^-) measurement of grafted and non-grafted NIL-T and NIL-S. The leaf Cl^- content **(a)** and Cl^- concentration **(b)** of reciprocally grafted, self-grafted, and non-grafted NIL-T and NIL-S was measured under salt stress (100 mM NaCl) for 8 days. The root Cl^- content **(c)** was measured under same conditions. n = 6-11. Asterisks indicate a significant difference between NIL 820-T and 820-S at $*p < 0.05$, $**p < 0.01$ according to the LSD test. T, NIL-T (*GmSALT3*); S, NIL-S (*Gmsal3*); ns, no significant difference.